LAWRENCE
LIVERMORE
NATIONAL
LABORATORY

UCRL-JRNL-207771

Experimental measurement of Au M-band flux in indirectly-driven double-shell implosions

H. F. Robey, T. S. Perry, H. S. Park, P. Amendt, C. M. Sorce, S. M. Compton, K. M. Campbell, J. P. Knauer

November 8, 2004

Physics of Plasmas

UCRL-JRNL-207771

Experimental measurement of Au M-band flux in indirectly-driven double-shell implosions

H. F. Robey, T. S. Perry, H.-S. Park, P. Amendt, C. M. Sorce,
S. M. Compton, K. M. Campbell
Lawrence Livermore National Laboratory, Livermore, CA USA 94550

J. P. Knauer
Laboratory for Laser Energetics, Rochester, NY

ABSTRACT

Indirectly-driven double-shell implosions are being investigated as a possible non-cryogenic path to ignition on the National Ignition Facility (NIF). In recent double-shell implosions, the inner shell trajectory was shown to exhibit a strong sensitivity to the temporal history of the M-band (2-5 keV) radiation emitted from the Au hohlraum wall. A large time-dependent discrepancy was observed between measurement and simulation of the x-ray flux in this range. In order to better characterize the radiation environment seen in these implosions, an experimental campaign was conducted on the Omega Laser. A number of diagnostics were used to measure both the temporal and spectral nature of the M-band flux. Results were obtained from an absolutely calibrated 12 channel filtered x-ray diode array (Dante) as well as two streaked crystal spectrometers and an absolutely calibrated time-integrated spectrometer (Henway). X-ray backlighting was also used to directly measure the effect of M-band radiation on the trajectory of the inner shell. The data from all diagnostics are shown to be in excellent agreement and provide a consistent picture of the M-band flux. These results are being used to improve the simulation of hohlraum-generated M-band radiation that will be necessary for the design of future double-shell implosions employing higher Z inner shells.

I. INTRODUCTION

Indirectly driven double-shell implosions are being investigated as a possible non-cryogenic path to ignition on the National Ignition Facility[1] (NIF). A NIF-scale double-shell capsule consists of two concentric spherical shells; a high-Z inner shell made of Au/Cu is used to contain the initial high pressure (790 atm) DT gas fill and provide enhanced radiation confinement at ignition time. A Cu-doped Be outer shell acts as the ablator, absorbing hohlraum-generated thermal x-rays and launching a double shock structure that compresses the inner shell leading to fuel compression and ignition[2]. A low-density (~10mg/cc) carbon foam is used to center the inner shell within the outer shell.

These targets provide an approach to ignition that is complementary to the more widely studied cryogenic single-shell designs[3-7]. Double-shell target designs present some new and formidable challenges, but also offer several unique advantages. The greatest advantage of this approach lies in the fact that double-shell capsules do not require cryogenic preparation, greatly simplifying the engineering required to field these designs. In addition, these implosions employ a relatively constant temporal profile of the hohlraum-generated x-ray radiation drive. This drive is generated using a laser pulse that delivers most of its energy to the hohlraum early in the pulse and relatively little later in time. Such a pulse shape minimizes plasma-induced backscatter from the ablated Au hohlraum walls, which fills the hohlraum at later time[2]. This is in marked contrast to the Haan pulse[4] proposed for cryogenic single-shell targets, which delivers the peak laser energy late in the pulse when backscatter can be the most problematical. The high-Z inner shell provides an additional advantage in that it provides strong confinement of radiation in the compressed fuel, thereby minimizing an additional energy loss mechanism from the compressing and igniting fuel.

These advantages come at a cost, however, with a corresponding list of new challenges to be addressed. The fabrication of double-shell targets is considerably more difficult than their single-shell counterparts, requiring precision micromachining and accurate assembly

of the various hemispherical shells. Targets employing lower density materials than those eventually required for ignition on NIF (CH vs. Au/Cu or Be) have recently been fabricated to the required precision[8] and have successfully been fielded on the Omega laser at the Laboratory for Laser Energetics, University of Rochester[9]. Several additional fabrication challenges remain, however, for the NIF ignition-scale targets.

Another major issue encountered in double shell research concerns the effect of capsule preheat due to high-energy x-rays emitted from the Au hohlraum walls. In particular, the 2-5 keV Au M-band radiation has been identified as a possible explanation for the observed low yield in some previous double-shell implosions[10]. These x-rays do not strongly affect the lower-Z outer shell. They are strongly absorbed, however, by the high-Z inner shell and can greatly affect the implosion characteristics. The understanding of high energy preheat and its temporal history is also of importance for achieving the precision shock timing required in cryogenic single-shell capsule implosions. A recent study by Olsen *et al.*[11] demonstrated that it is essential to accurately measure this x-ray source and include it in design simulations.

A clear example of the sensitivity of double shell performance to M-band preheating was observed in a recent series of implosion experiments on Omega[12]. In these experiments, a large time-dependent discrepancy was observed between measurement and simulation of the x-ray flux in the 2-5 keV region. This is shown in Figure 1(a). The measured flux, obtained with an absolutely-calibrated 10-channel filtered x-ray diode array (Dante)[13], is seen to be reasonably constant in time. In Figure 1(a), the 2-5 keV flux is given as a fraction of the total x-ray flux. The corresponding numerical simulation performed using the radiation-hydrodynamics code, Lasnex[14], by contrast, shows a greatly reduced M-band fraction early in time and a sharp increase in the middle of the pulse. The comparison between measurement and simulation of the full radiation drive history, by

contrast, shows good agreement[2]. The discrepancy between measurement and simulation only appears in the high-energy portion of the spectrum.

This uncertainty in the level of the M-band preheat has a significant consequence for the resulting yield from the implosion. This is shown in Figure 1(b), where the ratio of the experimentally measured yield over the clean, calculated yield (YOC) is shown for a wide range of implosions, both single and double shell. The YoC is plotted as a function of the "fall-line" parameter[2], a measure of the effect of mix on the implosion. If one assumes that the Dante measurement of Figure 1(a) is correct, the YOC of the double shells is of order 15-35%, a value very comparable to a wide range of previous single-shell implosions of similar convergence. If, on the other hand, the simulated temporal history of the M-band flux is correct, then the yield ratio is significantly lower, with a YOC of order 8-16%, noticeably below the corresponding value for single-shell implosions. In Figure 1(b), the experimentally measured yield is the same in both cases, but the simulated yield depends strongly on the level of preheat of the inner shell. The higher level of M-band preheat seen in the Dante measurement at early time causes a greater volumetric expansion of the inner shell as compared with the lower simulated preheat. This inner shell expansion reduces the efficiency of the implosion and the resulting neutron yield.

It is therefore very important to understand this preheat source and ascertain whether it is being measured or predicted correctly. Future double-shell implosion experiments will use inner shells made of materials of higher atomic number, and this issue will become increasingly more important. An accurate prediction of the performance of these double-shell capsules requires an accurate quantification of the level of M-band preheat. This is the goal of the present paper. A new series of experiments are reported employing several additional diagnostics to measure the M-band flux for the laser drive used in double-shell implosions and to confirm its temporal history.

II. EXPERIMENTAL SETUP

In order to better characterize the radiation environment seen in these implosions, a focused experimental campaign was conducted on the Omega Laser. A number of additional diagnostics were used to measure both the temporal and spectral nature of the M-band flux. The absolutely calibrated 10-channel filtered x-ray diode array (Dante) previously used for the measurements shown in Figure 1(a) was augmented with an additional two channels filtered to improve the spectral resolution of the radiation flux in the 2-5 keV energy range. The previous high-energy channel of Dante (Channel 10) uses a filter comprised of 1.0 μm Fe, 0.65 μm Cr, and 4.5 μm of paralyene (CH at 1.11 g/cc). Its normalized response (including the diode spectral response function) is shown in Figure 2 from 1 - 5 keV. This channel transmits a reasonable fraction of the energy over this entire range with a peak response at 2.9 keV. The transmission of the two new channels added to Dante is shown in Figure 2 as well. Channel 13 uses a 66 μm Saran ($C_7H_8Cl_{13}$) filter, which cuts off at 2.8 keV, and channel 14 uses a 4.5 μm Ag filter with an edge at 3.3 keV.

In addition, the present experiments also employed two time-resolved crystal spectrometers to measure both the temporal history as well as the spectral distribution of the hohlraum radiation flux. Both spectrometers used Rubidium Acid Phthalate (RAP) crystals with a 2d lattice spacing of 26.12 $\mathring{A}$. One of the crystals was flat, giving a nominal spectral range of 2.5-3.5 keV ($3.54\,\mathring{A} < \lambda < 4.96\,\mathring{A}$), and the other was curved to cover the energy range from 1.6-3.6 keV ($3.44\,\mathring{A} < \lambda < 7.75\,\mathring{A}$). Both were coupled to x-ray streak cameras using gold photocathodes, and the data was recorded onto film.

Since the radiation flux in the M-band originates principally from the locations where the laser beams hit the hohlraum wall[10], it is important to compare the views seen by the various diagnostics. The geometry of the experiment and the diagnostic views is shown in Figure 3. Figure 3(a) gives a CAD illustration of the overall target and beam geometry. The hohlraum was 2500 μm in length and 1600 μm in diameter. The x-ray drive was

provided by 20 beams entering each of the two laser entrance holes (LEH). The color of the beams corresponds to their angle with respect to the hohlraum axis. In each LEH, there are 5 beams at 21.4° (red), 5 beams at 42.0° (green), and 10 beams at 58.8° (blue). The beams are pointed and focused to achieve maximal symmetry of the x-ray drive as seen by the capsule[12]. On a small number of shots, a thin (5 μm) Sc backlighter foil was mounted on the hohlraum wall and illuminated by an additional six Omega beams, delayed in time, to radiograph the trajectory of the inner shell. On these backlit shots, 50 μm thick Ta shields were mounted on each end of the hohlraum. These shields, with an outer diameter of 7.5 mm and an inner diameter of 1.4 mm, were used to block the direct view of the 4.3 keV Sc backlighter x-rays from any of the principal diagnostics while allowing a clear view of the hohlraum LEH.

Figure 3(b) shows the view of one LEH as seen by Dante. The initial laser spot shapes and locations on the inside of the hohlraum are shown. Laser spots from all three cones are seen by Dante. The spectrometers were oriented so that they viewed the hohlraum from the same nominal angle as Dante (37.38° from the hohlraum axis of symmetry). The two spectrometers, each viewing one of the two LEHs, see a very similar beam pattern as shown in Figure 3(c), so their measured responses should be quite comparable to Dante. The data from the spectrometers will also be compared with measurements from an absolutely calibrated, high resolution, time-integrated spectrometer (Henway)[15]. This diagnostic views the hohlraum LEH from 63.43°, and therefore will see a somewhat different magnitude of the x-ray flux than the other diagnostics as shown in Figure 3(d). The spectral structure, however, should be comparable.

For most of the shots, the hohlraum was empty. For a small number, however, capsules were mounted in the hohlraums. On some of these shots, single plastic (CH) shells filled with 20 atm of DD and 0.1% Ar were used. The x-ray emission from the Ar in the hot core was imaged through a 400 μm diameter diagnostic access hole (seen in Figures 3(b, c)) using a gated x-ray framing camera to determine the implosion timing and symmetry. On

several other shots, a "diagnostic" double shell was used with x-ray backlighting to provide the implosion trajectory (radius vs. time) of the inner shell. On these capsules, an over-sized outer shell of polystyrene (CH) was used to filter out most of the thermal x-rays, allowing primarily the higher energy M-band x-rays to drive the implosion of a CH-coated glass inner shell. The glass strongly absorbs the higher energy x-rays, allowing for a direct measure of the effect of M-band radiation at the center of the hohlraum.

III. EXPERIMENTAL RESULTS

Figure 4 shows an example of the data from the one of the two spectrometers. We will focus in this paper on the data from the spectrometer (SSC-A) with the curved RAP crystal, which provided the larger spectral range. In Figure 4, the data has been corrected for the nonlinear response of the film, the transmission response function of all filters (3.5 to 6 mil Be, varying between shots), and the response function of the Au photocathode[16]. The spectral energy scale has been calibrated by performing several shots with a Saran filter giving a Cl K-edge cutoff at 2.8 keV. The spectra were also compared with published data[17] on Au M-band spectra to correct for the nonlinearity introduced by the crystal curvature. The temporal response of the streak camera was calibrated using a series of UV fiducial pulses on a separate shot. The absolute calibration of the flux is obtained by scaling to the temporally integrated 2-5 keV Dante channel 10 measurement value. In Figure 4, the abscissa is time in nanoseconds, and the ordinate is spectral energy in keV. The driving laser pulse (nominally 15 kJ in total energy) was 2.3 ns long, with a peak intensity of 10 TW for the first 0.5 ns followed by a monotonically decreasing intensity (see Figure 2 of Ref. 12 for a plot of the laser pulse). This pulse shape is designed to produce a relatively constant thermal x-ray flux in the hohlraum, and as seen in Figure 4, the flux in the 1.6 - 3.6 keV region is relatively constant in time as well.

Figure 5 shows a plot of the temporally integrated spectrometer data over the measured energy range. The absolute magnitude of the spectral intensity (J / keV-sr) for

the spectrometer data was provided by scaling the temporally and spectrally integrated data to the temporally integrated channel 10 measurement of Dante. Several broad dominant peaks are seen in the spectrum at 2.1, 2.5, 2.8, and 3.3 keV. These can be compared with the higher resolution measurements from the Henway instrument, an absolutely calibrated, temporally-integrated spectrometer. This diagnostic contains several crystals to cover a wide spectral range. In Figure 5, data is shown from a flat KAP crystal, filtered with 25 μm Be to cover the spectral range from 2.0-3.6 keV. Since the Henway views the LEH from a steeper angle than either Dante or the streaked spectrometers, a correction needs to be made to account for the geometry. This correction is provided by post-processing the numerically simulated hohlraum flux from Lasnex to obtain the flux seen at 37.38° and 63.43° from the hohlraum axis. This analysis gives a reduction in the magnitude of the x-ray flux by a factor of 1.8 at the Henway location as compared to the Dante or spectrometer locations. The assumption that the radiation goes as the cosine of the viewing angle gives a very similar correction factor of 1.78. This factor has been applied to the Henway data in Figure 5. For the purpose of comparing the two spectra, the Dante-scaled SSC-A data has been multiplied by an additional factor of 1.3 in Figure 5. The agreement between the two spectra is very good, both in the spectral structure as well as the absolute magnitude of the fluxes, which are within 30%. Considerably more detail in the spectral structure is seen in the Henway data due to the higher resolving power ($E / \Delta E \approx 4000$) compared to the lower resolution of the SSC-A ($E / \Delta E \approx 700$). The streaked spectrometer data thus provides a nice cross-calibration between two absolutely calibrated instruments. When all filter transmission functions and geometric correction factors are applied, the absolute fluxes seen by Dante and Henway are in very reasonable agreement as Figure 5 demonstrates.

Turning now to the temporal response, Figure 6(a) shows a comparison of the spectrally integrated streak camera data with the corresponding Dante measurements for five successive Omega shots. The data from several shots is shown to assess the repeatability of the measurements. Different filter thicknesses were used on each shot to enhance the

photon statistics in various portions of the spectrum. In this Figure, the spectrometer data has been filtered with the Dante channel 10 spectral response function shown in Figure 2, convolved with the Dante temporal response function, and scaled in absolute value to match the temporally-integrated flux seen by Dante. Taking into account the unusually large shot-to-shot variability in the pulse shapes and laser energy (10%), the overall repeatability of the temporal history of the M-band flux is very good. There is considerable variation in the peak flux, but in all cases the flux history is much flatter than that given by the simulation in Figure 1(a).

In Figure 6(b), a subset of the data is shown to more directly compare the result of the two diagnostics with that of the simulation. For this plot, the average flux is shown for two shots (#35457 and #35458), both of which used empty hohlraums with no possibility of any additional radiation from either backlighting or capsule emission. The flux history for both Dante and SSC-A are relatively flat and exceed the simulated flux by a factor of two for the first half of the pulse. The agreement of these two diagnostics confirms that the experimental measurement of the M-band flux shown in Figure 1(a) is indeed correct and that the simulated time history is in error. This also confirms that the YoC of these double-shell implosions is consistent with that observed for a wide range of single-shell implosions as seen in Figure 1(b).

The one consistent difference between the two diagnostics as seen in Figure 6(a, b) is the appearance of two distinct peaks in the spectrometer data, one at $t \approx 1$ and one at $t \approx 2$ ns, whereas the Dante response shows a relatively flat response early in the pulse (still well above the simulation) with a single peak at approximately 2 ns. This early peak just barely exceeds the error bars on the Dante data in Figure 6(b), but is somewhat greater in several of the additional shots shown in Figure 6(a). The effect of this small discrepancy on the capsule performance, as determined by numerical simulations using either the Dante or the SSC-A M-band measurements, however, is very small.

A possible explanation for this difference comes from the very broad spectral filter used in Dante channel 10. As Figure 2 shows, the spectral response of Dante channel 10 extends considerably beyond the range covered by the spectrometer. A more direct comparison between the two diagnostics can be obtained from the two additional Dante channels (13 and 14), which provide more narrow spectral resolution than channel 10. Figure 7 shows a comparison of the absolute flux of these three channels from both diagnostics. Each plot again gives the average of two shots (#35457 and #35458). The spectrometer data is obtained by convolving with the appropriate Dante spectral response functions of Figure 2. For all three channels, the agreement between the two diagnostics is quite good. A slight peak at $t \approx 1$ ns is now evident in both Dante channels 13 and 14, giving a somewhat flatter overall temporal response in better agreement with the spectrometer data.

This slight difference in response of the three Dante channels can be better understood by further examination of the spectral response of the spectrometer. In Figure 8, the temporal history of the flux is plotted for four broad sub-regions of the spectrometer data. The four spectral bins (each 400 eV wide) are chosen to contain the dominant M-band spectral peaks seen in Figure 5 at 2.1, 2.5, 2.8, and 3.3 keV. The curves in Figure 8 are normalized to a peak of one to account for the differing energy in each of these spectral bins. Shown for comparison is the normalized Dante channel 10 history. The spectrometer data from 2.3-2.7 keV exhibits a very distinct early-time peak. The other three bins, by contrast, show an early-time response that is equal to or less than that of Dante channel 10. This helps to explain why channel 10 does not resolve this early peak, as it averages over all of these spectral bins as well as including even higher energy contributions. Channels 13 and 14, by comparison, have a narrower spectral response, which sees a greater relative contribution from the M-band transitions around 2.5 keV.

The measurements discussed thus far have all been obtained externally from radiation emitted from the hohlraum LEH. On one shot (#35464), an additional diagnostic

was employed to measure the effect of the M-band radiation directly on the inner shell of a double shell capsule. The capsule was a diagnostic double shell with no fuel to provide any neutron yield. The capsule had an over-sized outer shell of CH, whose primary purpose was to filter out the bulk of the thermal x-ray flux allowing the higher energy M-band x-rays to drive the implosion of a CH-tamped glass inner shell. The implosion trajectory of the inner shell was imaged with a Sc backlighter foil, which was mounted on the hohlraum wall and illuminated by an additional 6 beams of Omega using the same pulse shape, but delayed in time relative to the drive by 1.5 ns. The absorption images of the inner shell were analyzed to provide the capsule radius vs. time. This trajectory is plotted in Figure 9 for both shot # 35464 and a previous shot (#31549), which imaged a similar diagnostic double shell capsule at earlier time. In both cases, the radius is defined by azimuthally averaging radial lineouts of the backlighter transmission through the inner shell and identifying the location of the transmission minimum. Error bars on the radial positions are estimated by taking the radial locations at which the transmission is 5% greater than this minimum value.

Lasnex simulations of the inner shell trajectory are shown for comparison. The individual capsule dimensions and laser drive histories were used for each of the two shots in separate simulations. The dashed curves give the trajectory obtained using the "standard" M-band simulation, which as seen in Figures 1(a) and 6(b) were low by a factor of 2-3 for the first half of the pulse. The solid lines give the trajectory simulated using an M-band source scaled to match the temporal history of the Dante channel 10 measurement. This curve is in much better agreement with the data. This provides a more direct measurement of the effect of the M-band source on the double shell implosion trajectory. This measurement, together with the Dante, SSC-A, and Henway data provide a consistent picture of the hohlraum generated M-band x-rays for this pulse shape.

IV. DISCUSSION

The data from this series of experiments provide an unambiguous picture of the temporal history of M-band x-rays generated using a reverse-ramp laser pulse shape. The issue now becomes the identification of the source of the error in the simulation of this flux. A practical interim solution has been demonstrated in Figure 9, where time-dependent emissivity multipliers have been applied to the Au hohlraum wall in order to force the simulations to match the M-band flux as measured by Dante or the SSC-A. This results in simulated implosion trajectories, which are in agreement with the radiographic data. A more thorough solution, however, will require improvement in the atomic physics in the code. This effort is underway, and the results will be reported in a forthcoming publication.

V. ACKNOWLEDGEMENTS

This work was performed under the auspices of the U.S. Department of Energy by the University of California, Lawrence Livermore National Laboratory under contract No. W-7405-Eng-48.

VI. REFERENCES

[1]J. A. Paisner, J. D. Boyes, S. A. Kumpan, W. H. Lowdermilk, and M. S. Sorem, *Laser Focus World* 30, 75 (1994).

[2]Peter Amendt, J. D. Colvin, R. E. Tipton *et al*., *Phys. Plasmas* **9**(5), 2221 (2002).

[3]J.D. Lindl, Inertial Confinement Fusion (*Springer-Verlag, New York, 1998*).

[4]S.W. Haan, S. M. Pollaine, J. D. Lindl *et al*., *Phys. Plasmas* **2**, 2480 (1995).

[5]D. H. Munro, P. M. Celliers, G. W. Collins, D. M. Gold, L.B. DaSilva, S. W. Haan, R. C. Cauble, B. A. Hammel, and W. W. Hsing, *Phys. Plasmas* **8**, 2245 (2001).

[6]S. M. Pollaine, D. K. Bradley, O. L. Landen, R. J. Wallace, O. S. Jones, P. A. Amendt, L. J. Suter, and R. E. Turner, *Phys. Plasmas* **8**, 2357 (2001).

[7]L. J. Suter, J. Rothenberg, D. Munro, B. Van Wonterghem, and S. W. Haan, *Phys. Plasmas* **7**, 2092 (2000).

[8]R.L. Hibbard *et al*., Fusion Science Technology, to appear (2004).

[9]T. R. Boehly, D. R. Brown, R. S. Craxton *et al*., *Opt. Commun.* **133**, 495 (1997).

[10]W. S. Varnum, N. D. Delameter, S. C. Evans *et al*., *Phys. Rev. Lett* . **81**, 5153 (2000).

[11]R. E. Olsen, R. J. Leeper, A. Nobile, and J. A. Oertel, *Phys. Rev. Lett.* **91**, 235002 (2003).

[12]Peter A. Amendt, Harry F. Robey, H.-S. Park *et al*., *Phys. Rev. Lett.*, in submission (2004).

[13]H.N. Kornblum, R.L. Kauffman, and J.A. Smith, *Rev. Sci. Instrum*. **57**, 2179 (1986).

[14]G. B. Zimmerman and W. L. Kruer, *Comments Plasma Phys. Controlled Fusion* **2**, 51 (1975).

[15]L. N. Koppel and J. D. Eckels, *LLNL document* UCRL-79781 (1977).

[16]B. L. Henke, J. P. Knauer, and K. Premaratne, *J. Appl. Phys*. **52**(3), 1509 (1981).

[17]Robert Kauffman, in Handbook of Plasma Physics, Vol. 3: Physics of Laser Plasma, Eds. A. M. Rubenchik and S. Witkowski (*North-Holland, Amsterdam*, 1991).

VII. FIGURE CAPTIONS

Figure 1. (a) Comparison of the measured M-band fraction with the nominal Lasnex simulation for Omega shot #31551. (b) Difference in the measured-to-predicted neutron yield ratio of a double-shell implosion resulting from the simulated vs. the measured M-band x-ray flux.

Figure 2. Normalized x-ray response function of the three high-energy channels (10, 13, 14) of Dante.

Figure 3. (a) CAD illustration of the target and beam geometry with 40 beams for indirect drive and 6 time-delayed backlighter beams for radiography. View of the laser entrance hole (LEH) and initial beam spots on the inside hohlraum wall as seen by the three principal diagnostics, (b) Dante, (c) temporally-resolved crystal spectrometer (SSC-A), and (d) Henway.

Figure 4. Temporally resolved x-ray spectrum from Omega shot #35457.

Figure 5. Comparison of the spectrometer data with an absolutely-calibrated, temporally-integrated spectrometer (Henway). The Dante-scaled SSC data is multiplied by a factor of 1.3 for comparison.

Figure 6. (a) Comparison of the flux histories of Dante and SSC-A for five successive shots using different filtering on the spectrometer data. (b) Comparison of Dante and SSC-

A flux histories with the corresponding Lasnex simulation. Data are averaged over two shots (#35457 and #35458) using empty hohlraums.

Figure 7. Comparison of the temporal response of Dante channels 10, 13, and 14 with the correspondingly filtered and spectrally integrated data from SSC-A.

Figure 8. Comparison of the temporal history of the M-band flux from four discrete energy bins taken from the spectrometer data.

Figure 9. Trajectory of the inner shell of a diagnostic double shell obtained by backlit x-ray radiography. The dashed curves give the trajectory predicted by the nominal Lasnex simulations, and the solid curves give the simulations using an M-band temporal history scaled to match the Dante measurement.

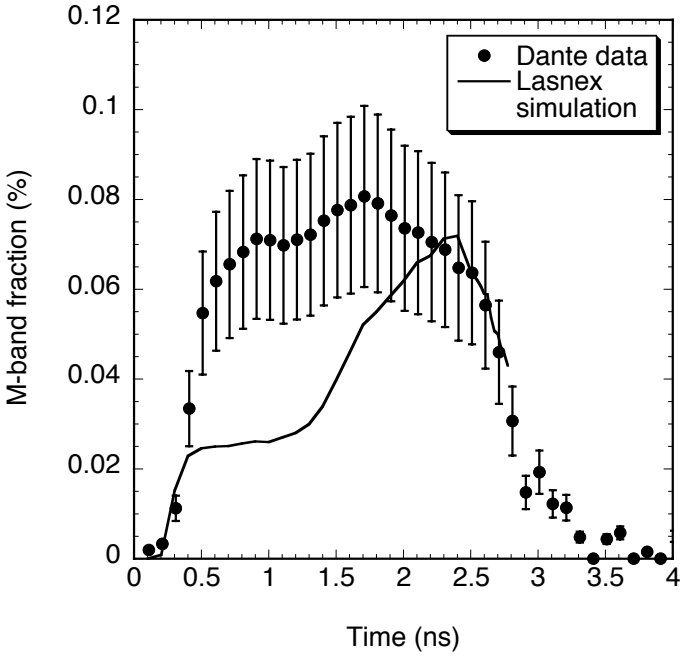

(a)

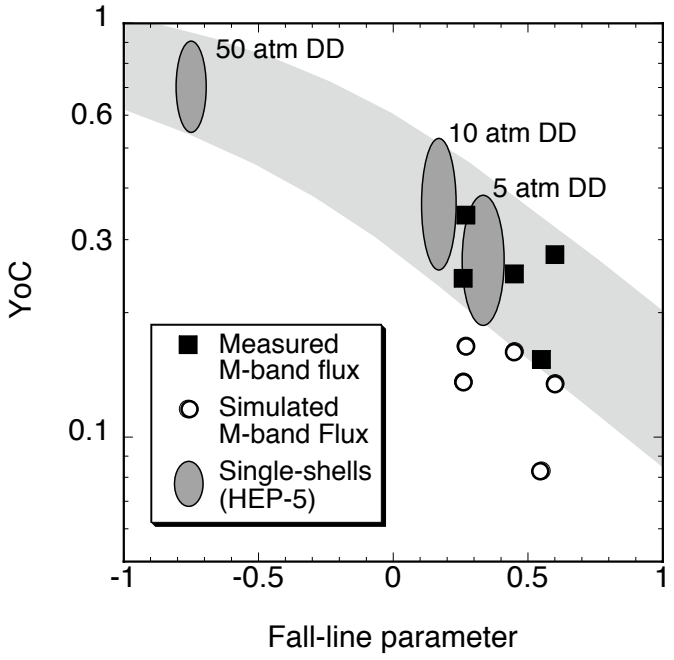

(b)

Figure 1, Robey *et al.*, Phys. Plasmas

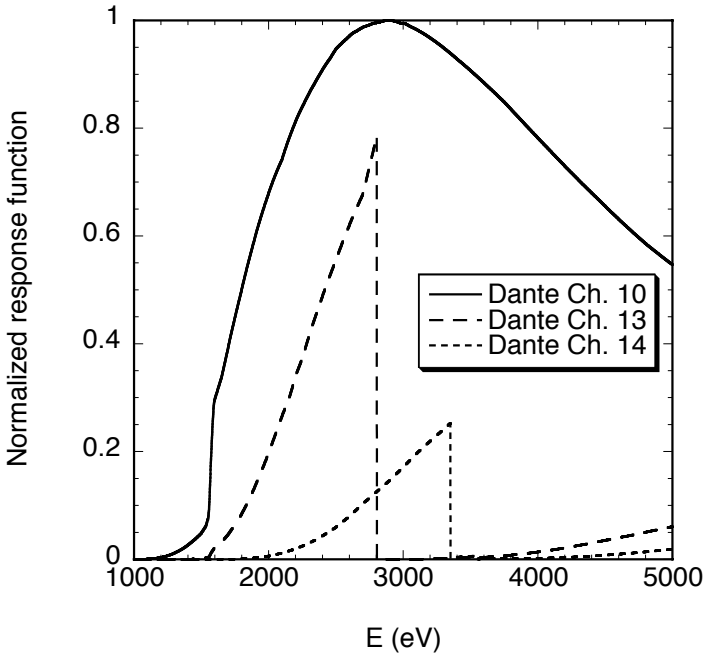

Figure 2, Robey *et al.*, Phys. Plasmas

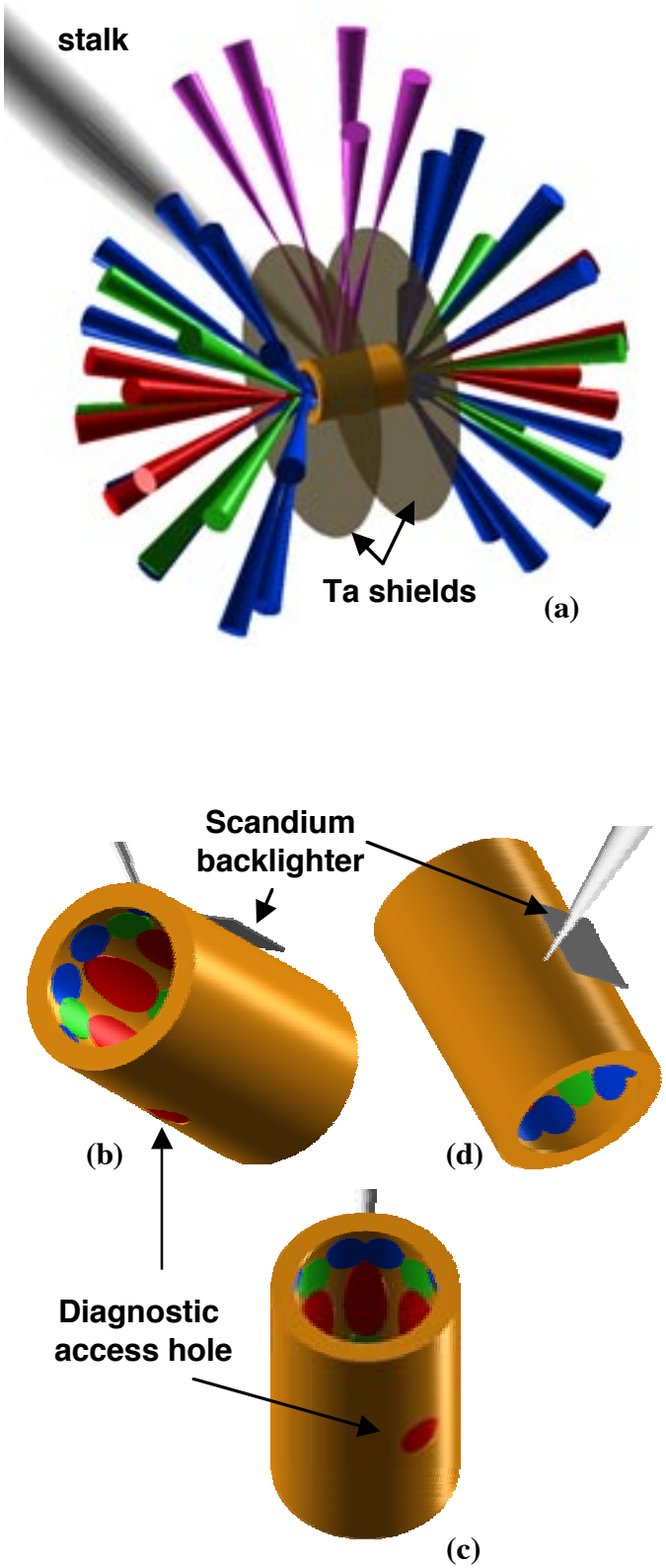

Figure 3, Robey *et al.*, Phys. Plasmas

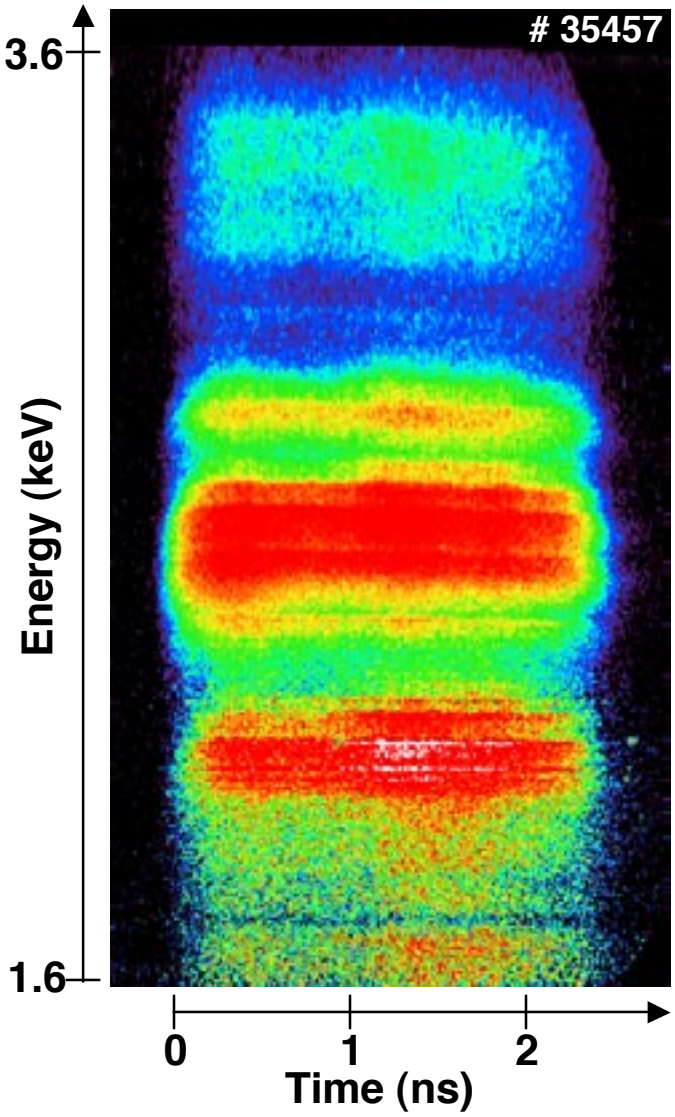

Figure 4, Robey *et al.*, Phys. Plasmas

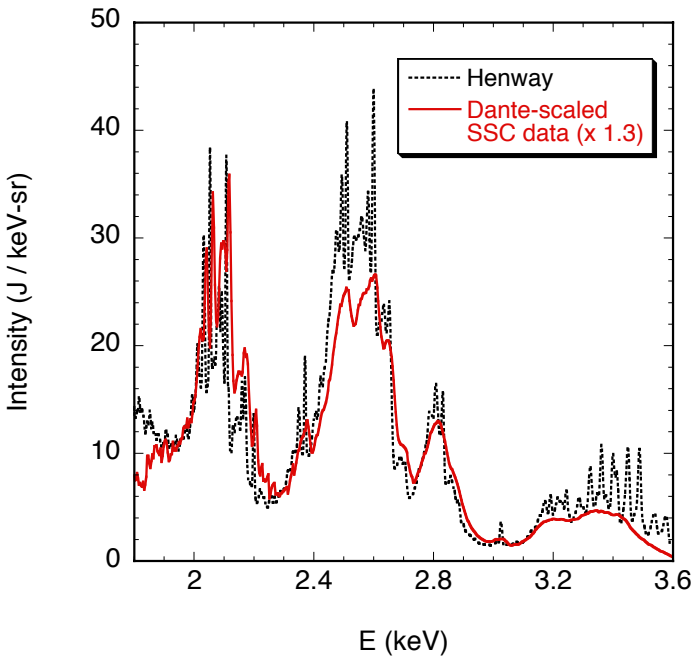

Figure 5, Robey *et al.*, Phys. Plasmas

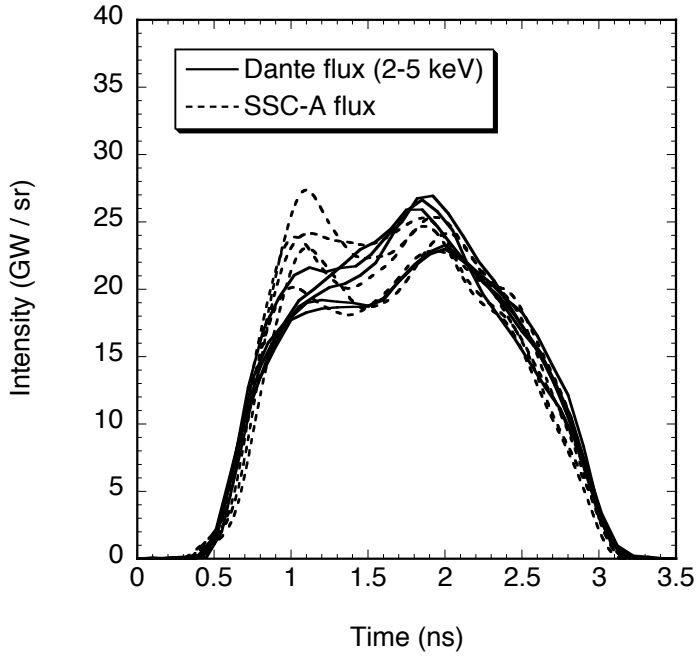

(a)

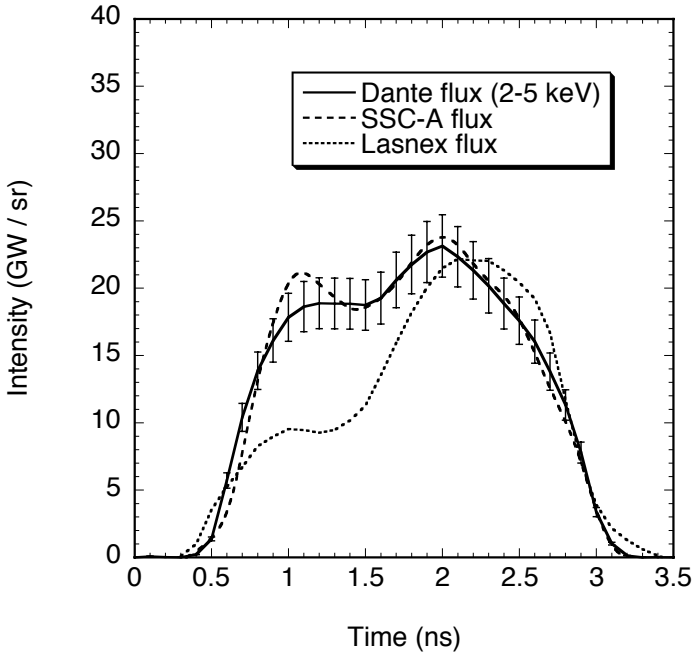

(b)

Figure 6, Robey *et al.*, Phys. Plasmas

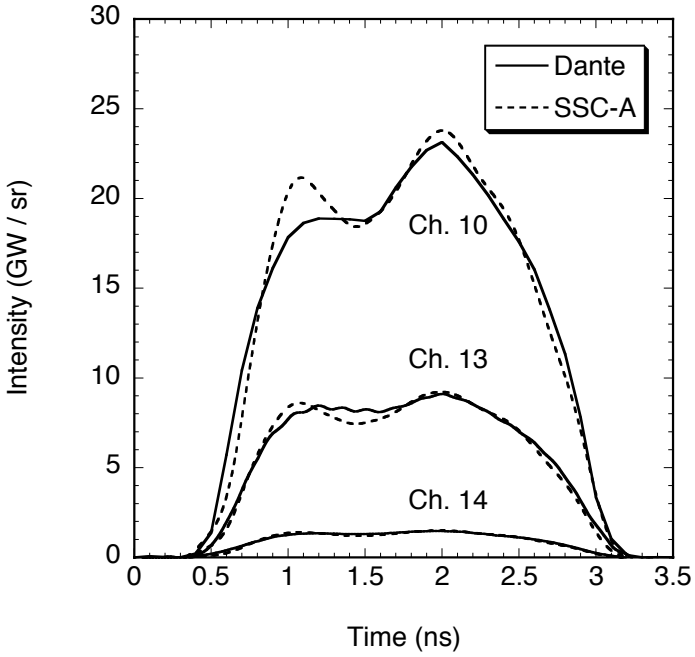

Figure 7, Robey *et al.*, Phys. Plasmas

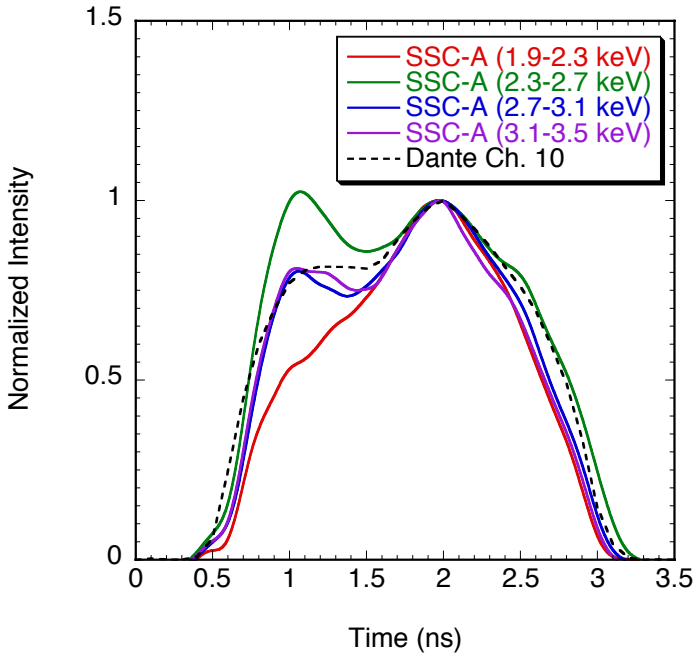

Figure 8, Robey *et al.*, Phys. Plasmas

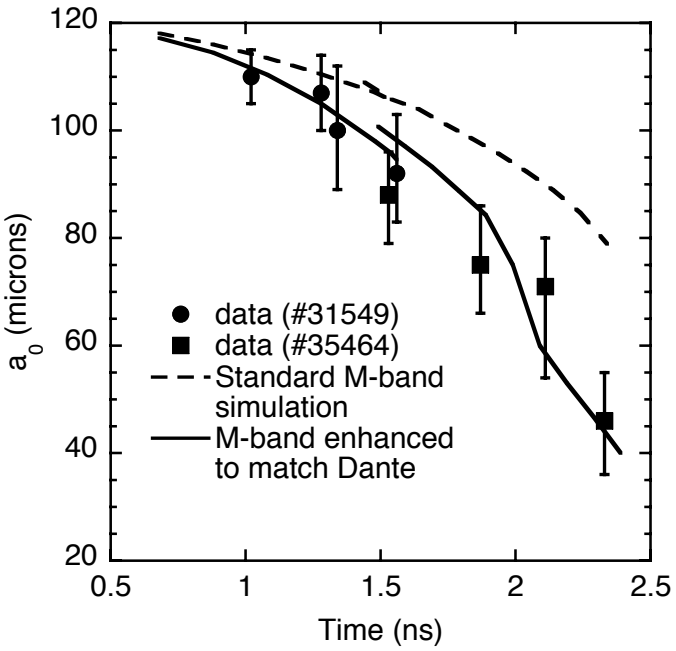

Figure 9, Robey *et al.*, Phys. Plasmas